Modeling the percutaneous absorption of solvent-deposited solids over a wide dose range: II. Weak electrolytes

Kevin Tonnis[a], Joanna Jaworska[b], Gerald B. Kasting[c*]

[a]College of Engineering and Applied Science
The University of Cincinnati
Cincinnati, OH USA 45221

[b]The Procter & Gamble Company
Data and Modeling Sciences
Brussels Innovation Center, Belgium

[c]The James L. Winkle College of Pharmacy
The University of Cincinnati
Cincinnati, OH USA 45267-0514

[*]Correspondence:

Gerald B. Kasting
The James L. Winkle College of Pharmacy
University of Cincinnati Academic Health Center
Cincinnati, OH 45247-0514
Phone: 01 513-558-1817
Email: Gerald.Kasting@uc.edu

Abstract

Dermal absorption of weak electrolytes applied to skin from pharmaceutical and cosmetic compositions is an important consideration for both their efficacy and skin safety. We developed a mechanistic, physics-based framework that simulates this process for leave on applications following solvent deposition. We incorporated this framework into our finite dose computational skin permeation model previously tested with nonelectrolytes to generate quantitative predictions for weak electrolytes. To test the model, we analyzed experimental data from an in vitro human skin permeation study of a weak acid (benzoic acid) and a weak base (propranolol) and their sodium and hydrochloride salts from simple, ethanol/water vehicles as a function of dose and ionization state. Key factors controlling absorption are the pH and buffer capacity of the dose solution, the dissolution rate of precipitated solids into a lipid boundary layer and the rate of conversion of the deposited solid to its conjugate form as the nonionized component permeates and (sometimes) evaporates from the skin surface. The resulting framework not only describes the current test data but has the potential to predict the absorption of other weak electrolytes following topical application.

Keywords: buffer capacity, mathematical modeling, percutaneous absorption, skin, weak acid, weak base

1. Introduction

The theory of finite dose absorption of pharmaceutical compounds following solvent deposition on skin has been addressed multiple times dating back to early experimental work and analysis thereof by Scheuplein and Ross [1]. For low doses that dissolve into the upper stratum corneum (SC) or for compounds that are either liquid at skin temperature or dissolve rapidly into the skin, elegant analytical solutions to this problem have been found [2-6]. Anissimov and Roberts provide an excellent summary up to 2001 as well as impressive fits to Scheuplein's data [4]. The matter becomes thornier when the solute precipitates on the skin surface or in the upper SC. Delivery in this case may become dissolution-limited, and dissolution kinetics can be complex [7, 8]. We recently addressed this problem in order to model the finite dose absorption of two small nonelectrolytes, niacinamide and methyl nicotinate [9]. A dissolution-limitation was proposed for niacinamide, whereas methyl nicotinate appeared to dissolve rapidly on the skin, or perhaps never even crystallized.

An extension to the above problem is presented by the case in which the dissolved solute is a weak electrolyte, and the composition of the deposited solute is governed by the ionization state of the solute in the formulation. This case is of practical interest for dermatological drugs such as diclofenac and lidocaine, which are commonly formulated at a neutral pH in which the bulk of the active agent is ionized. The magnitude of the dose and the rate at which the pH of the SC returns to its natural value of 5.0-5.5 presumably govern the delivery rate of the drug to the lower skin layers and beyond. A second case of interest is the finite dose testing of cosmetic ingredients for their dermal absorption characteristics, either to assess their potential for delivering skin benefits or systemic absorption. Toxicologists often eschew the addition of extra

excipients to test formulations and may recommend compositions that mimic internal body conditions. Interpreting absorption of weak electrolytes tested under these conditions can be challenging [10]. Some guidance is offered by steady state analyses of weak electrolyte absorption from aqueous solutions as a function of pH [11-14], which have shown that the skin permeability of weak acids and especially weak bases do not conform to the pH-partition hypothesis for lipid membrane permeability. However, these analyses apply to dilute solutions and do not involve a dissolution step, so they are not directly applicable to the solvent deposition scenario. Particularly detailed, mechanistic finite dose simulations of topical application of two weak acids, diclofenac and benzoic acid have been recently published by FDA and Certara scientists [15, 16]. These simulations were conducted on Certara's Symcyp platform with the MPML MechDermA™ extension, a modeling framework that has the capability of modeling precipitation and redissolution of dissolved and potentially ionizable solutes. The issues of formulation and SC pH and their respective buffer capacities were clearly recognized by these authors. Patel et al. write "It is unclear whether the skin surface pH or the formulation pH are responsible for the fraction nonionized at the skin surface, therefore the simulator allows the user to select which of these values is used for the calculation. Currently, the interplay between these two and their buffering capacities is not modeled," later adding "The interplay between buffering capacities of the skin and formulations is still largely unknown." The research reported here addresses this issue.

In this report we discuss the underlying mechanisms that drive cutaneous permeation of finite dose applications of weak electrolytes dissolved in volatile solvents and provide an update to the model developed within our group [9, 10]. The resulting model describes the

percutaneous absorption of weak electrolytes over the full range of ionization states and skin loads that might be encountered in topical products. The model, which we term Model 4.1 following the nomenclature introduced in [10], is calibrated for in vitro exposures by analyzing a previously published experimental study from our group involving benzoic acid (BA, a weak acid) and propranolol (PR, a weak base) [17]. New features not incorporated in our previous analyses nor, to our knowledge, reported elsewhere include (1) an exponential return of SC pH to its natural value following topical application, with a time constant proportional to the buffer capacity of the dose solution; (2) a load-dependent fractional contact area of the deposited solid with the skin; and (3) a slow transfer of protons across the lipid dissolution layer that allows gradual conversion of precipitated salt to free acid or base, enabling continuous permeation of the deposited solute. We acknowledge that application of the developed model to in vivo exposures will likely involve substitution of a skin surface lipid film for the SC lipid film as discussed by Yu et al. [9] and also an upward adjustment of the skin buffer capacity as discussed by Miller and Kasting [17]. Nomenclature associated with the analysis is summarized in Table S1 of the Supplementary Information (SI).

The solvent-deposited solid problem is a subset of the more general problem of the dry down of semisolid products on skin, a field that has recently been dignified by substitution of the word “metamorphosis” for “dry down”. Aspects of this process have been studied for many years, as recently reviewed by Jin et al. [18]. The area has received considerable attention in recent years due to the interest from the US FDA and dermatological drug manufacturers in facilitating generic topical drug approvals by establishing robust in vitro bioequivalence measures. A series of FDA workshops have been held on this subject, e.g. [19-21] and successful

examples of generic approvals are now available [15, 16]. Research continues in both experimental method development and simulation and modeling of the dry down process.

2. Methods

2.1 Experimental dataset

We analyzed results of a study by Miller and Kasting which was designed to provide insight to transient penetration of weak acids and bases over a wide range of pH and skin load [17]. This was an in vitro human skin permeation study of BA and PR and their sodium and hydrochloride salts, respectively, using radiochemical methods. The test compounds were delivered to unoccluded skin from aqueous ethanol with dose volumes ranging from 5-20 μL. Five combinations of each acid/conjugate base pair ranging from pure acid (or base) to pure conjugate base (or acid) were tested at four logarithmically spaced doses. Measurements included permeation into the receptor fluid (RF) from 0 to 72 h and distribution into the skin wash, epidermis (ED) and dermis (DE) at the end of each experiment.

Physical properties of the test permeants at 25°C were reported in Ref. [17]. We made several changes and additions to the data reported there that included (1) correcting vapor pressures (P_{vp}) to 32°C and changing the units to Pascals; (2) distinguishing between the vapor pressure of the solid and the subcooled liquid as in [9]; (3) estimating the fraction of each solute unbound to albumin in the VE and DE according to ACD Laboratories software [22]; and (4) estimating the activity coefficients of each solute in a binary mixture with water using COSMOthermX 2021 software [23]. Sodium benzoate and propranolol HCl have P_{vp} values more

than five orders of magnitude lower than their conjugates, so they were assumed to have a P_{vp} of zero in the simulations. A table of revised parameters is included in Table S2.

2.2 Mathematical model for weak electrolytes

The mathematical model employed in this study builds upon a model developed by our group to simulate finite dose absorption of potentially volatile and/or ionizable compounds [9, 10]. It is a multilayered one-dimensional transient diffusion/evaporation model built on the gPROMS platform to simulate the disposition of compounds applied to the surface of skin. The model incorporates a vehicle layer, a lipid dissolution layer at the skin surface, three skin layers including stratum corneum (SC), viable epidermis (ED), and dermis (DE), as well as a parallel diffusion pathway through hair follicles. Its steady state behavior with compounds over a wide range of lipophilicity, molecular weight and ionization state has been thoroughly explored [14, 24]. Recently, modeling capability for transient applications has been enhanced through the addition of an enhanced binary evaporation and dissolution model for deposited solids (Model 3) [9], and a transient keratin binding model (Model 4.0) [10]. Further features added to the model to describe the transient behavior of weak electrolytes over a wide range of skin load, pK_a and formulation pH and buffer capacity are described in the Appendix. We will call the revised model Model 4.1. An illustration of the surface/SC interface of Model 4.1 is shown in Fig. 1.

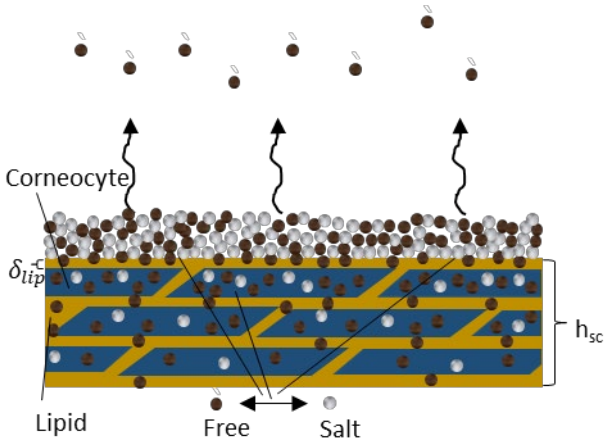

Fig. 1. Schematic illustration of the surface/SC interface of a weak electrolyte deposited on skin in a partially ionized state. The surface roughness depicted in Yu et al. 2022 [9] is still present, but has been omitted here for clarity.

2.3 Model settings and parameters

2.3.1. Ambient conditions and dose properties

Simulation parameters were set to match the conditions of the experiments performed by Miller and Kasting [17]. The experiments were performed in a fume hood, so the gas phase mass transfer coefficients (k_g, Eq. (A8)) were calculated using an air flow rate u = 0.5 m/s as in [10]. This choice is somewhat less than the value u = 0.92 m/s estimated by Gajjar et al. [25] for this same apparatus and our older default value of u = 0.72 m/s for outdoor or fume hood exposures [26]. The reason for this choice is related to the frequently seen large masses of precipitated solute on the skin and is discussed in Sect. 4.4.

Miller and Kasting dosed BA and its salts in a 1:1 v/v ethanol:water mixture and PR and its salts in a 3:1 v/v ethanol:water mixture. These are clearly ternary mixtures comprised of two solvents plus the weak electrolyte. For simulations, ethanol was assumed to quickly evaporate so the dose solution could be represented as a binary mixture. This approximation was required as a practical matter (the computer code was limited to one- and two-component vehicles), but

it is also justified by previous measurements of ethanol disposition on skin in our laboratory. Ethanol was one of the solvents used for calibration of the evaporation model [25], and was later shown to conform closely to this model over the dose range 5-40 mg/cm^2 [27]. Notably, ethanol cleared completely and rapidly from the skin in the latter study, with no evidence of binding to the tissue. Further details regarding ethanol evaporation rate and skin disposition in the 2014 study are recently discussed by Xu and Kasting [28], who also employed this solvent system. The initial pH of the doses with only the neutral form of each permeant, i.e. 100% BA or 100% PR.HCl, was calculated as [29]

$$\mathrm{pH} = 0.5[\mathrm{p}K_a - \log(C_a)] \quad (1)$$

whereas that of doses with only the base, i.e. 100% Na benzoate or 100% PR, was calculated as

$$\mathrm{pH} = 0.5[\mathrm{p}K_a + \mathrm{p}K_w + \log(C_a)] \quad (2)$$

The pH of doses containing a mixture of free acid or base and its salt were calculated as

$$\mathrm{pH} = \mathrm{p}K_a - \log\left(\frac{C_a}{C_b}\right) \quad (3)$$

We recognize that these are approximate equations for dilute aqueous solutions, but the effort to calculate activity coefficients and the impact of ethanol on the effective pH was not warranted given the rapid dry down of these formulations. The most important factor in the simulations was the initial ratio of neutral and salt forms of the permeants. Table S3 lists the total amount and calculated initial pH and buffer capacity (β_{dose}) of each dose. It is provided also as a spreadsheet so the manner of calculating β_{dose} can be examined.

Accurate estimation of BA evaporative loss over a wide range of dose and ionization state required careful attention. Slow conversion of salt to free acid on the surface was implemented as described in Sects. A.5 and A.6. Newly formed free acid beneath a layer of salt exceeding 50 nmol·cm^{-2} was considered to not evaporate due to occlusion by the salt (Sect. A.6). Because the lowest dose for BA was small compared to the amount that can be dissolved in the top layer of the SC [5], Na benzoate deposited under these conditions was assumed to not occlude the surface, and free acid formed by slow conversion of the salt at the surface according to Eqs. (A15-A17) was considered to be subject to evaporative loss. For the larger doses, we considered that enough salt remained on the surface to prevent evaporation at this stage of the experiment. These considerations did not apply to propranolol, which was essentially nonvolatile in either ionization state.

2.3.2. Skin properties

The skin properties used in the simulations were set to represent the experimental conditions in Ref. [17] combined with diffusion model defaults [30, 31]. The total skin thickness was set at 400 μm, with a 100 μm ED and an SC thickness of 13.365 μm for partially hydrated skin and 43.365 μm for fully hydrated skin. For all but one of the simulations, the skin was assumed to be partially hydrated. For the largest dose of BA and its salts (which employed a 20 μL dose volume containing 10 uL of water), the fully hydrated skin model was employed as discussed in Sect. 4.3. For the latter doses, the flux into the SC after the solvent was no longer present on the surface (approximately 2 to 11 min, depending on dose and vehicle composition) was reduced by a factor of three to mimic the return of the skin to its partially hydrated state. This was accomplished by a three-fold reduction in the value of $f_{contact}$.

Miller and Kasting employed posterior leg skin obtained from five donors. We simulated this tissue using the model default hair follicle density of 24 hairs·cm^{-2}, a density that corresponds with broad body surfaces [14, 32]. The impact of follicle density is discussed in Sect. 4.5.

2.3.3. Fitted parameters

As noted in the Introduction, the subject of pH drift in the SC following topical applications and its relationship to SC buffer capacity is not well understood. There are many reports of skin surface pH drifting back to the natural SC value over a period of several hours after product application and also a small body of work from Maibach and coworkers on pH drift in the SC following application of strong acids and bases [33-35]. The latter is discussed in the SI. We found the Maibach work to be informative, but not directly applicable to weak electrolyte applications where a portion of the dose may precipitate on the skin surface following application. As an alternative we proposed the pH evolution presented in Sects. A.1 and A.5, which combined the concepts of dose buffer capacity, SC buffer capacity, neutralization of precipitated salt and evaporation of free acid (or base) to describe both short term pH recovery and long term release from precipitated weak electrolytes. In order to do this, we fit two parameters to the experimental data, a_0 in Eq. (A1) and a_1 in Eq. (A17). We also adjusted one boundary condition at the vehicle/SC interface as described at the end of this section.

According to Eqs. (A1) and (A4), the time constant for pH recovery in the SC in the absence of competing phenomena depends on the SC buffer capacity, β_{sc}, the dose buffer capacity, β_{dose}, and a proportionality constant, a_0. We assumed β_{sc} = 10 nmol·cm^{-2} [17], calculated β_{dose} (Table S3) and then adjusted a_0 by repeatedly simulating all doses (and all ionization states) of both BA

and PR. The optimum fits were a_0 = 1.5 h^{-1} and 3.0 h^{-1}, respectively. These values were not significantly different according to visual estimation, and BA was more sensitive to changes in a_0 than PR, so we took a_0 = 2 h^{-1} (5.6 $\times$ 10^{-4} s^{-1}) as a suitable compromise. There is experimental basis for expecting that the product $a_0\beta_{sc}$ to be different for acids and bases as discussed in the SI, but the present analysis lacks the sensitivity to firmly establish this difference.

According to Model 4.1, the proportionality constant a_1 in Eq. (A17) determines the rate at which protons from the SC lead to interconversion of salt and free acid or base deposited on the skin surface. This is evidently a slow process and was evaluated in a manner similar to a_0. The process has a smaller effect on large doses where a slow change between salt and free acid or base is small compared to the overall amount of solid. Although every dose was observed, only the simulations of smaller doses appreciably changed by varying a_1. PR.HCl has a pH close to that of skin for most of the experiment, so it was not sensitive to changes in a_1, and the BA value of 1.0 $\times$ 10^{-6} nmol $cm^{-2}s^{-1}$ was close to an optimum fit, so it was used for both compounds. We are not aware of a theoretical basis for why a_1 should differ for acids and bases, although the neutralization rate should clearly take into account the valence of the electrolyte as proposed in Eq. (A17).

It was found that free BA and PR deposited as solids permeated the skin quite efficiently, with no evidence of the dissolution limitation suggested by Eqs. (A10-A11). This result was similar to our previous finding for methyl nicotinate applied to skin in an identical manner [9]. Consequently, we replaced Eqs. (A10-A11) with a boundary condition expressing partition equilibrium between a saturated solution of BA or PR and the surface of SC while solid free acid

or base was present. Thus, $C_{sc}(0,t) = C_{sat}$ during this time, where $C_{sat} = K_{sc/w} \cdot S_w$ is the solubility of the permeant in the SC [5]. Here $K_{sc/w}$ is the SC/water partition coefficient at the relevant hydration state and S_w is the water solubility of the permeant. Using the terminology introduced in [9], we thus considered free BA and PR to be "soft solids", whereas their salt forms were taken to be "hard solids", cf. Eqs. (A12-A13).

2.3.4. Evaluation of model performance

We calculated two statistics associated with the Model 4.1 fit to the permeation into the receptor fluid (RF) of each test compound. Both were based on an unequal variance model in which the weight of each observation was related to its standard error according to $w_i = 1/\mathrm{SE}_i^2$ [36]. This weighting scheme was chosen due to the large variation in SE between the various doses and ionization states. The first was an adjusted squared correlation coefficient (R^2) calculated as

$$\overline{\mathrm{R}}^2 = 1 - \frac{\mathrm{SS}_{res}/\mathrm{df}_{res}}{\mathrm{SS}_{tot}/\mathrm{df}_{tot}} \tag{4}$$

where

$$\mathrm{SS}_{res} = \sum_i w_i [y_i(\mathrm{obs}) - y_i(\mathrm{calc})]^2 \text{ ; } \mathrm{df}_{res} = n - p - 1 \tag{5}$$

$$\mathrm{SS}_{tot} = \sum_i w_i [y_i(\mathrm{obs}) - \bar{y}]^2 \text{ ; } \mathrm{df}_{tot} = n - 1 \tag{6}$$

Here $\bar{y}$ is the average value of the dependent variable, n is the number of observations and p is the number of parameters adjusted to create the fit. The second is a quality of fit parameter that Bevington termed χ_v^2, defined as [36]

$$\chi_v^2 = \frac{1}{n-p} \cdot \mathrm{SS}_{res} \tag{7}$$

Values of χ_υ^2 close to 1 indicate that the model reproduces the experimental data to within experimental error. Larger values are indicative of systematic error, whereas smaller values suggest overfitting of the data.

3. Results

Figure 2 shows the cumulative experimental and simulated permeation of BA, PR and salts thereof across human skin in vitro for each of the four logarithmically-spaced doses. Thus, small doses of the nonionized compounds permeated well and large doses of fully ionized compounds permeated very poorly. As noted by Miller and Kasting [17], large doses of the nonionized compounds permeated better than expected from simple finite dose absorption models. Since the vehicles evaporated within 2 to 11 min according to the simulation, it is clear that solutes deposited in either ionized or nonionized form continued to permeate from the solid state.

The overall adjusted R^2 for the fit to the BA data calculated according to Eq. (4) was $\overline{R}^2$ = 0.965 and the associated quality of fit parameter (Eq. (7)) was χ_υ^2 = 2.43. The latter result indicates that some systematic error remained, which is evident from a study of Fig. 2a. These results were based on n = 140 observations (4 doses $\times$ 5 ionization states $\times$ 7 time points) and p = 6 adjustable parameters. Three of the parameters were associated with evaporation rate adjustments, one (a_0) with pH recovery time, one (a_1) with proton transfer rate and one (soft solid approximation, Sect. 2.3.3) with dissolution rate. There are many more parameters in the underlying model; however, these were determined by earlier calibrations and were not varied in Model 4.1.

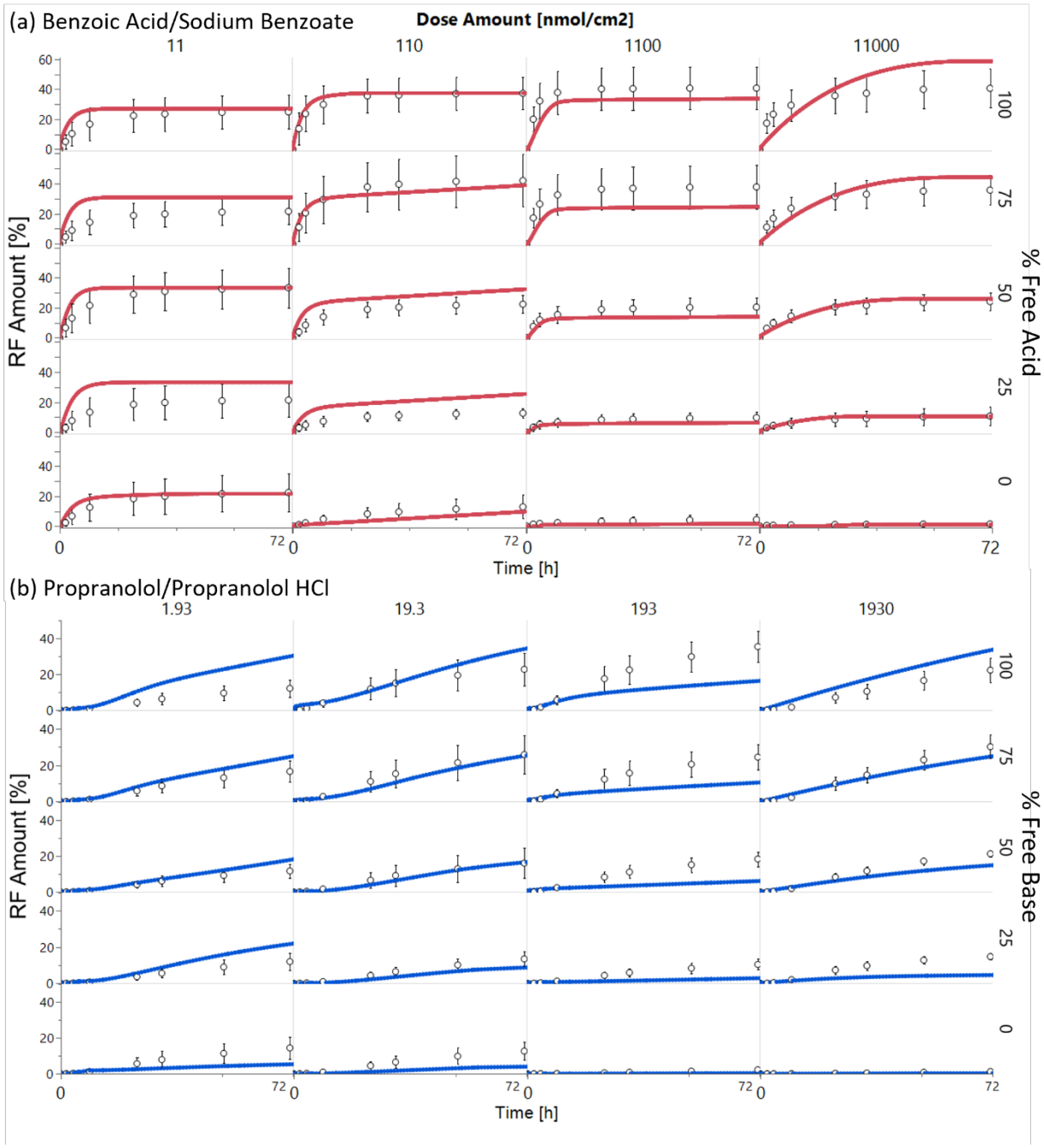

Fig. 2. Experimentally measured RF amounts (open circles) and simulated RF amounts (solid lines) for (a) benzoic acid/sodium benzoate and (b) propranolol/propranolol HCl. Dose increases from left to right and percent free acid or base increases from bottom to top.

Statistics for the weighted fit to the PR data were heavily influenced by the first two time points (2h and 4h post-dose), where less than 1% of the dose had permeated yet experimental error was even lower. These data contributed greater than 80% of the weighted variance, yet

their practical significance was negligible, cf. Fig. 2b. A better assessment of model fit was achieved by considering only the data from 9-72 h post-dose. The overall adjusted R^2 for the fit to the PR data over this time frame was $\overline{R}^2$ = 0.998 and the quality of fit parameter was χ_υ^2 = 7.45. Thus, there was more systematic error for PR than for BA. This difference was largely due to smaller experimental error at low doses and lower degrees of ionization. It is likely that the lack of volatility of PR free base led to more precise experimental results vs. the more volatile BA free acid. These results were based on *n* = 100 observations (4 doses × 5 ionization states × 5 time points) and *p* = 3 adjustable parameters (evaporation was inconsequential for PR).

The difference in absolute amounts of both compounds absorbed across doses is enormous, as shown for free acid and base forms in Fig. 3. The early time simulations of PR permeation (Fig. 3b) show very rapid absorption of small amounts of the free base that was not observed experimentally, since the first RF collection time was 2 h post-dose. In Model 4.1, this absorption is due to follicular delivery. We note also that simulation of BA permeation at a dose of 11000 nmol·cm^{-2} was improved by switching to a fully hydrated skin model, whereas this change was not indicated for 1930 nmol·cm^{-2} of PR. This difference may be attributed to the fact that the high dose BA formulation contained 10 μL of water, whereas high dose PR contained only 5 μL of water.

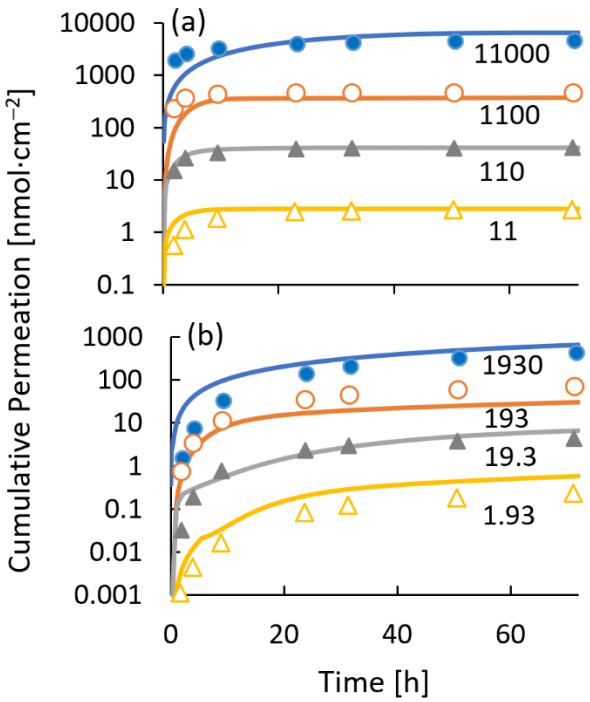

Fig. 3. Cumulative permeation data from Fig. 2 replotted in terms of absolute amounts permeated into the RF for (a) 100% free benzoic acid; (b) 100% propranolol base. The numbers associated with the data are the specific dose in nmol·cm^{-2}.

The percent of dose evaporated in the experiments for BA is compared with the simulated values in Fig. 4. Neither the experiment nor the simulation showed large amounts remaining in any layer of the skin after 72h. For PR the mass balance was stated by Miller and Kasting [17] to be 86-106% for the individual treatments, with an average across all treatments of (94.3 ± 5.5)%. This is close to the recovery target in OECD 428 (2004)[37] of 90-110% for non volatile compounds, and also about as high a recovery as we tend to generate in our laboratory with our volumetric dosing technique. We take this result to indicate that there was no significant evaporative loss of ^{14}C-PR in this study, consistent with its low vapor pressure (Table S2).

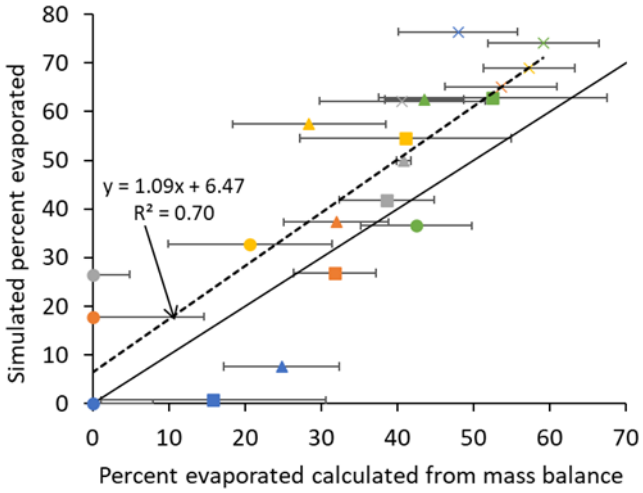

Fig. 4. Percent of dose evaporated for benzoic acid formulations dosed at 11000 nmol cm^{-2} (circles), 1100 nmol·cm^{-2} (squares), 110 nmol cm^{-2} (triangles) and 11 nmol cm^{-2} (×) with 100% free acid (blue), 75% free acid (orange), 50% free acid (gray), 25% free acid (yellow) and 0% free acid (green). The solid black line is the line of perfect fit, and the dashed line is a linear regression. Experiments with over 100% recovery are shown as 0% evaporated.

4. Discussion

The analysis presented here reinforces how difficult it is to predict transient skin absorption phenomena from arbitrary topical applications of a wide variety of chemicals, even with a complex model. We have had the experimental data considered here for several years. We published them without analysis in 2022 [17] as a guide to an ongoing computational analysis of finite dose absorption of cosmetic-relevant chemicals [10]. Our group had previously analyzed several dose-ranging studies of the dermal absorption of nonelectrolytes including both volatile liquids [5, 26, 38] and solids [9, 39]. Following the most recent analyses, we considered that we were finally in a position to quantitatively analyze this dataset, which includes a weak acid and a weak base, dosed from simple solvent systems over a wide range of skin loads and ionization states. But the analysis was still difficult.

The interplay between skin and dose buffer capacity, skin pH and hydration state, and the dissolution and evaporation rates of solutes deposited on the skin surface was complex. We explored several scenarios seeking one that could simultaneously handle all of these phenomena. The scenario presented here includes the following new features not present in our previous models, nor (to the best of our knowledge) in the myriad modeling alternatives that have sprung up in the past decade: (1) a skin pH recovery time that depends on both the SC buffer capacity and the pH and buffer capacity of the applied dose; (2) a slow transfer of protons or carriers thereof between the skin and weak electrolytes deposited as solid particles on the skin surface; (3) a hydration state of the skin that depends in a novel way upon the amount of water contained in the dose solution and its evaporation rate; and (4) a change in saturated vapor pressure of volatile chemicals applied to the skin depending on their state of solution on the skin surface. These factors are explored in the discussion below. We realize that the solution presented here may not be unique and offer in the SI a summary tabulation of the experimental permeation values to allow others to try their hand at improving upon the present analysis (Table S4).

4.1 Skin pH recovery time

According to Model 4.1, the pH of the entire SC adopts that of the dose solution immediately following a topical application. The SC and dose solution pH then drift exponentially back to the natural pH of the SC with a time constant given by Eqs. (A1-A4). For small doses the recovery time can be seconds or a few minutes, whereas for large ones it can be many hours. Table 1 shows half-lives for SC pH recovery for the permeants and doses applied in the Miller and Kasting study [17], calculated from Eqs. (A1-A4). It should be noted that the half-lives longer than a few hours are hypothetical for in vivo exposures, as other processes intervene. In such

situations, skin sloughing, product rub off or product wash off occur after several hours and surface deposits are removed. However, the shorter half-lives are plausible and may help to explain why topical drugs such as diclofenac or lidocaine are effective when dosed as salts at low application levels.

Table 1

Estimated half-lives (h) for SC pH recovery for the experiments in [17][a]

Benzoic Acid	% free acid				
Dose, nmol cm^{-2}	100[b]	75	50	25	0
11000	362	268	173	77	17.8
1100	36.0	26.8	17.3	7.7	1.8
110	3.53	2.68	1.73	0.77	0.18
11	0.33	0.27	0.17	0.077	0.018
Propranolol	% free base				
Dose ,nmol cm^{-2}	100[b]	75	50	25	0
1930	66	50	33	16.7	4.9E-03
193	6.6	5.0	3.3	1.67	2.8E-04
19.3	0.64	0.50	0.33	0.17	3.8E-05
1.93	0.058	0.05	0.03	0.017	2.9E-06

[a]Calculated according to Eqs. (A1-A4) using the parameter values tabulated in Table S3.
[b]Values for these solutions calculated assuming entire dose stays in solution.

A different picture arises from analysis of the skin surface pH drift following application of strong acids and bases in vivo [33-35], as described in the SI. Here, the major effect of dose is the magnitude of the initial ΔpH, but the recovery time constant is independent of the applied dose. We speculate that the immediate neutralization of strong acids and bases in solution expected from chemical equilibrium combined with enhanced pH recovery kinetics in vivo [17] leads to different recovery kinetics from those of solvent-deposited weak electrolytes in vitro. This matter is certainly deserving of further scrutiny.

4.2 Impact of skin baseline pH on weak electrolyte permeation

As may be anticipated from Eqs. (A1-A4), the rate of SC pH recovery following a dose of weak electrolyte depends, in part, on the baseline (or natural) pH of the skin, $\mathrm{pH}_{sc}^{\infty}$. There is natural physiological variation in $\mathrm{pH}_{sc}^{\infty}$ ranging from about 4.0-6.0 [40] that depends on the individual and the skin site, with typical values in the range 5.0-5.5. Somewhat higher values have been reported for axilla (where it depends on sweating activity) [41] and for in vitro studies; for example, Zhai et al. [34] report $\mathrm{pH}_{sc}^{\infty}$ = 5.6-5.9 in the in vitro studies discussed in the SI to this report. In light of this variability and the fact that Miller and Kasting did not measure $\mathrm{pH}_{sc}^{\infty}$ of the SC samples yielding the data analyzed in this report, we conducted a sensitivity analysis for the predicted permeation results for BA and PR for $\mathrm{pH}_{sc}^{\infty}$ values ranging from 5.5-6.5. In interpreting these results, one must bear in mind that this analysis is specific for weak acids with pK_a values typical of carboxylic acids and weak bases with pK_a values typical of alkyl amines, as the difference between the pK_a of the weak electrolyte and $\mathrm{pH}_{sc}^{\infty}$ is central to the problem.

For BA, raising $\mathrm{pH}_{sc}^{\infty}$ tended to decrease the permeation rate; however, the effect was only significant at the lowest dose, 11 nmol cm^{-2}. Results are shown in Fig. 5a and Panels (a-d) of Fig. S4. At the 11 nmol cm^{-2} dose only, this effect was not monotonic (cf. Fig. 5a), with permeation slightly increasing for $\mathrm{pH}_{sc}^{\infty}$ = 6.0. Analysis showed the local maximum reflected the interplay between the ionization state of BA and its solubility in the SC.

For PR, permeation increased with increasing $\mathrm{pH}_{sc}^{\infty}$ (Fig. 5b and Panels (e-h) of Fig. S4). Significant increases were seen for doses in the range 1.93-193 nmol cm^{-2}. The increase was

greatest at the smallest dose and reflects the increasing fraction of PR free base at higher skin pH.

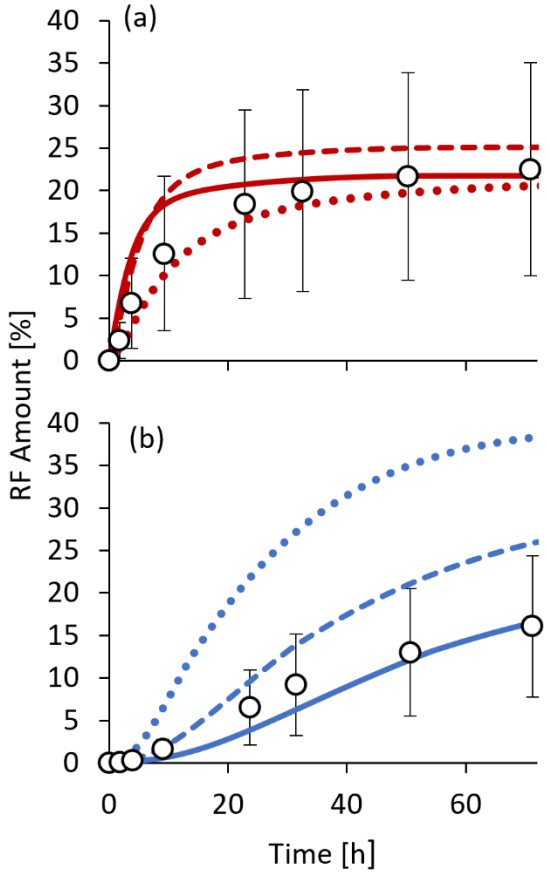

Fig. 5. Predicted impact of baseline SC pH (pH_{sc}^{∞}) on skin permeation of (a) 11 nmol cm^{-2} BA dosed as 0% free acid; and (b) 1.93 nmol cm^{-2} PR dosed as 50% free base. Curves represent pH_{sc}^{∞} values of 5.5 (solid lines), 6.0 (dashed lines) and 6.5 (dotted lines). Experimental values are shown as open circles.

4.3 Proton transfer between the skin and deposited solids

With or without a mathematical model to quantify the effect, it is evident that deposited solids in the Miller and Kasting study [17], including both neutral forms and salts, continued to penetrate into and through the skin well after the ethanol:water vehicle had evaporated. The penetration of nonionized, lipophilic solutes at low-to-moderate doses was adequately handled by our previous computational models that include a lipid dissolution layer at the SC/vehicle

interface [9, 10]; however, penetration of the salts was not. Tonnis et al. [10] assumed a "hard solid" limit for precipitated salts, i.e. no penetration for these materials once they had crystallized. This assumption created no issues given the low absorption and high amounts in skin wash for weak electrolytes in the dataset analyzed in that study.

In order to explain the permeation of deposited salts, a mechanism for slow dissolution of salt on the skin surface was required. We examined two – the proton transfer mechanism described in this report and an alternative scheme involving partially hydrated crystals with a microscopic aqueous film covering the surface of each particle. The latter concept has considerable precedent in the area of solid state stability [7, 8]. According to the film theory, crystalline solids slowly dissolve into the aqueous layer, where they are subject to more rapid degradative processes such as oxidation and hydrolysis. For the present skin disposition problem, the list of dissipative processes could include absorption and evaporation from such a surface film. However, details of the stability models are highly dependent on the specific surface area and hygroscopicity of the crystalline solid, as well as the relative humidity of the environment; thus, successful quantitative models tend to be compound- and polymorph-specific. For the present analysis, we had little or no data regarding the crystal properties or the possibility of co-crystallization of neutral and salt forms. Furthermore, the dissolution of BA or its sodium salt into an aqueous film led to the prospect of using subcooled liquid vapor pressure for the neutral species, leading to calculated evaporation rates much higher than those inferred from mass balance (Fig. 4). We eventually abandoned this scheme in favor of the simpler proton transfer concept.

Our present model for SC lipids, first described in [14], includes a small, size-selective aqueous pathway through the intercellular lipids we have attributed to either corneodesmosomes, lipid defects or a combination of both. Protons are highly mobile in aqueous environments due to a "hopping" mechanism between water molecules [42]; moreover SC lipid lamellae in the outer skin layers are already in a somewhat degraded state [43]. Thus, it is plausible that proton transport across the lipid dissolution layer in this model (assumed to be SC intercellular lipids for in vitro studies with thoroughly washed cadaver skin [9]) could be significantly faster than the transport of the much larger and less mobile ions present in weak electrolyte salts. The proton transfer postulate allows small amounts of deposited salts to be neutralized at the skin surface and to subsequently diffuse into the SC through the surface lipid layer, without invoking direct transport of the salt through either the aqueous channels or (by an ion pairing mechanism) directly through the SC lipids. Further investigation of this subject to identify the specific mechanism by which pharmaceutical salts deposited on the skin surface are gradually neutralized is warranted.

As implemented in Model 4.1, solute flux into the SC due to the proton transfer mechanism depends only the relative amounts of salt and free electrolyte on the skin surface, not on the total amount of solid deposited. Consequently, it has stronger impact for smaller doses. Simulations conducted with and without this mechanism in place are shown in Fig. 6 and Fig. S5. Proton transfer significantly impacted the RF kinetics of BA and PR only at the two smaller doses used in this study. We note that at the 11 nmol cm^{-2} dose, only a small amount of BA was predicted to precipitate on the skin surface, limiting the impact of proton leakage on the simulation. The largest impact was seen for BA when it was dosed as a salt and for PR when it

was dosed as a free base because those doses result in the largest pH gradient between the surface deposit and the SC. Figure 6 shows a comparison of predicted RF kinetics with and without the proton transfer mechanism for the doses with the largest difference. A comparison for every dose is shown in the SI (Fig. S5).

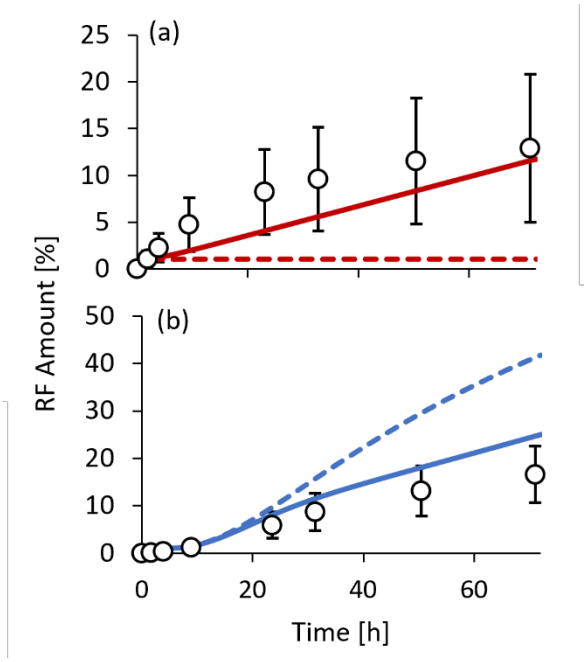

Fig. 6. Predicted impact of proton transfer mechanism discussed in Sect. 4.3 on skin permeation of (a) 110 nmol cm^{-2} BA dosed as 0% free acid, and (b) 1.93 nmol cm^{-2} PR dosed as 75% free base. Solid lines show the results with proton transfer implemented and dashed lines show those in the absence of proton transfer. Experimental values are shown as open circles.

4.4 Skin hydration state

In Model 4.1 and its predecessors tracing back to Wang et al. 2007 [30], skin hydration state impacts both partitioning of solutes into the SC and transport through it. Fully hydrated skin (SC water content ~78% w/w) is thicker and about three times more permeable than partially hydrated skin (SC water content ~30% w/w) according to current parameterization of the model. With one notable exception [44], all of these models limit the skin to these two distinct states and do not allow for a smooth transition during execution of the codes.

Partially hydrated SC is usually the state of choice for finite dose absorption studies on unoccluded skin. However, Tonnis et al. [10] adopted a fully hydrated model for the analysis of a subset of cosmetic ingredients tested in vitro by Cosmetics Europe and dosed from phosphate-buffered saline solution with a dose volume of 10 $\mu L \cdot cm^{-2}$. There was experimental evidence that these solutes penetrated skin rapidly and at rates more consistent with the hydrated skin model for the first few hours of the study; furthermore, evaporation rates estimated from solute mass balance in the Cosmetics Europe study were considerably lower than the default values calculated in our model. In the present analysis we employed a partially hydrated skin model for all test conditions except for the highest BA/sodium benzoate dose (11000 nmol cm^{-2}), which had a dose volume of 20 μL, 10 μL of which was water. The hydrated skin model provided a better fit to these data, although we dialed the permeability back down after several minutes as described in Sect. 2.3.2. We acknowledge that this modification was made on the basis of limited data, but it is certainly plausible that the hydration state may change with larger aqueous doses. If one adopts the skin thickness and water uptake parameters described in the skin swelling model of Li et al. [44] it is shown in the SI that as little as 3 $\mu L/cm^2$ of water, if completely absorbed into the skin, is enough to effect the transition from partially hydrated to fully hydrated SC for a period lasting some tens of minutes. The adjustment was not necessary for high dose PR/PR.HCl leg (1930 nmol cm^{-2}), for which the dose volume was also 20 μL, only 5 μL of which was water. Clearly, the incorporation of the transient swelling capability described in Li et al. [44] or an equivalent approach would be a valuable addition to the present model.

4.5 Vapor pressure and airflow considerations

Evaporation rates of both solvents and volatile solutes impact solute disposition following unoccluded topical applications. Although it is difficult to predict these values exactly under uncontrolled conditions, solute and solvent evaporation are linked by common environmental factors. Common ways of handling this involve evaporation and gas phase mass transfer coefficients, k_{evap} and k_g, cf. Eqs. (A7) and (A8).

The vapor pressure (P_{vp}) of the species of interest has a direct impact on k_{evap}. Choosing the correct vapor pressure is critical to the success of the calculation. Vapor pressures of crystalline solids are considerably less than those of subcooled liquids (which are often calculated by physical properties estimation programs such as EpiSuite™). The two are related by a relationship given by Haftka et al. [45] which is employed in our model [9]. Vapor pressures are also directly proportional to the activity of the solute (or solvent) in solution, a fact that is highly relevant during the dry down process. We used a commercial thermodynamics package (COSMOthermX [23]) to estimate the activities of both solute and solvent during this critical stage of absorption.

Wind velocity (or airflow), u, as well as geometry and molecular weight, contribute to the gas phase mass transfer coefficient, k_g. The dependence of k_g on u depends upon the nature of the airflow. For laminar flow, analytical solutions yield $k_g \sim u^{0.5}$ [46]. For turbulent flow, numerical simulations yield an average close to $k_g \sim u^{0.78}$. We continue to apply a turbulent flow model deriving from a US EPA chemical spills model [47], i.e. Eq. (A8), to Franz cell data, as we have calibrated this model to our diffusion cell system [25] and also have concerns regarding the application of laminar flow models to the Franz cell geometry. Closely related heat and mass

transfer calculations suggest turbulence and even oscillations in such a geometry [48, 49]. Frasch and Bunge provide a thorough discussion of the EPA model and present a laminar flow model developed with in vivo exposures to the human hands in mind [46]. We recommend their model for in vivo exposures, but believe the jury is still out regarding in vitro data from Franz cells or related diffusion cell systems.

In the present analysis we selected an airflow value of u = 0.50 m·s^{-1} as in Tonnis et al. [10], as it led to a better fit to the calculated evaporation in the BA study (Fig. 2a) than higher values previously estimated for our apparatus, cf. Sect. 2.3.1. We hypothesize that BA evaporation rates for the higher doses were slowed by the accumulation of large amounts of precipitated solid on the skin surface, lowering the effective evaporation mass transfer coefficient. We considered accounting for this effect with a dose-air contact factor analogous to $f_{contact}$ in Eq. (A11) but lacked sufficient data to do this in a convincing manner. This is another example of the many ways experimental conditions can impact evaporation rates.

4.6 Impact of polar pathway (hair follicles and micropores)

Model 4.1, as well as its immediate predecessors [9, 10], implements a polar pathway through the SC consisting of two components – an appendageal or hair follicle pathway and a system of micropores through the SC lipid lamellae. These components permit the entry of ions and large hydrophilic molecules into the SC and subsequent permeation through the tissue. It is instructive to see how the presence of these components impacts the skin permeation of BA and PR as the model is presently constituted.

Fig. 7 shows simulations of the cumulative permeation of BA and PR for a single dose and ionization state in the presence and absence of the polar pathway model components. The data for a low dose of each compound in its 100% free acid or free base form are shown. There is a stark difference between the two compounds – the polar pathway had little impact on BA permeation (Fig. 7a), but a large impact on PR permeation. Most of the latter was due to the micropore component rather than the hair follicles. The difference can be attributed to the much larger nonionized fraction (f_{non}) of BA than PR at and near the natural pH of the SC. For example, at pH 5.5, f_{non}^{BA} = 0.047, whereas f_{non}^{PR} = 1.2×10^{-4} (Table S3). The presence of several percent

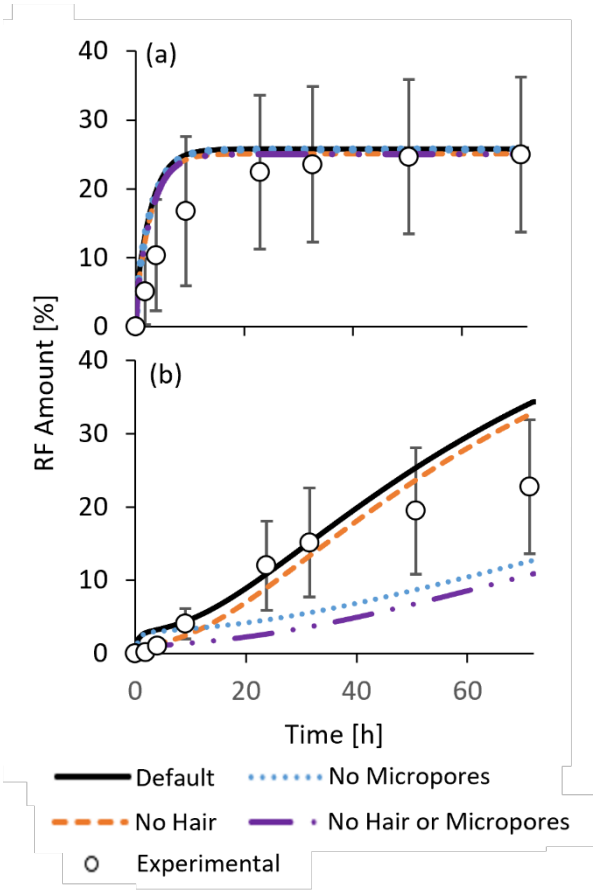

Fig.7. Simulations showing the impact of polar pathway components on the cumulative permeation of a low dose of nonionized permeant. The experimental data and the default simulations are those in the top left or second-to-left panels of Fig. 2. (a) 11 nmol cm^{-2} BA; (b) 19.3 nmol cm^{-2} PR.

of nonionized BA during the dry down period leads to rapid permeation of BA through the SC lipid/corneocyte composite matrix [30], whereas PR permeation via this route is limited due to the low diffusing concentration of the free base.

4.7 Targeted and controlled delivery for leave-on applications

Model 4.1 allows formulators to gain insights for controlled release and targeted delivery of weak electrolytes. The model can help to quantify SC pH kinetics, and predict not only delivery phenomena that are currently studied using empirical trial-and-error approaches but also internal fluxes that are not possible to measure in the physical world. The main controlling formulation factors for delivery are electrolyte pK_a, pH, buffer capacity and dose. They determine ionized and nonionized mass fractions in the formulation, as well as mass fractions of free electrolyte and its salt form on the skin surface, which have 3-4 orders of magnitude different penetration rates according to Model 4.1. The SC pH decays to baseline exponentially based on the initial formulation pH and its buffer capacity relative to that of the SC. This decay, in turn, determines the rate of salt formation and dissolution. These complex time dependencies render the model particularly useful for quantitative guidance that goes beyond qualitative principles known to formulators.

In the discussion below we treat the salt as an inactive form and consider the free acid or base form to be the active one.

4.7.1 Dermal/systemic delivery insights

To maximize systemic delivery, dosing electrolytes in their free or nonionized forms is optimal if they are soluble. For moderate-to-highly soluble materials highly ionized at pH 5.5 high buffer capacity is recommended; examples include α- or β-hydroxy acids (pK_a 2.8-3.8), where

absorption of large doses with correspondingly high buffer capacities is greatly facilitated at low pH [50, 51]. For soluble materials substantially nonionized at pH 5.5 low buffer capacity is acceptable. In both cases these strategies maintain the permeation rate as the pH recovers to baseline.

For sparingly soluble weak electrolytes at low to moderate doses, using salt is a better strategy as it increases solubility and results in increased partitioning into the aqueous phase of the SC. Successful examples of this approach include topical diclofenac sodium [16] and other diclofenac salts [52]. In addition, for volatile compounds, using salt prevents loss due to evaporation. However, there is a watch out. If the salt dose is larger than the amount required to saturate the deposition layer of the SC, the benefit in improved partitioning will be offset by the lower mobility of the salt compared to the free form. Once deposited on the surface, salt takes longer to penetrate the skin than free acids and bases because what is already in the deposition layer of the SC must first diffuse into lower layers, which takes longer for the ionized permeant. Salt must also convert to its free form before the initial penetration to the SC, making it slower than deposited free acids or bases.

4.7.2 Surface and SC as the target

For some ionizable over-the-counter drugs, e.g. the antimicrobial chlorhexidine gluconate, it is desirable to minimize skin penetration. The strategies to achieve this are the inverse of strategies to maximize delivery beyond the SC.

5. Conclusions

In this study, we attempted to advance understanding of how weak electrolytes and their salts penetrate skin after finite dose applications from simple, volatile vehicles. We built a mathematical framework for predicting how the pH will change over time within the SC after dosing and how pH affects the dissolution and penetration of deposited solids into skin. Using that framework, we were able to reproduce the in vitro human skin penetration of a weak acid and a weak base over a wide range of initial pH and dose sizes. Our analysis highlights how formulation pH and buffer capacity directly impact cutaneous absorption. If the formulation pH is not carefully considered, a wide range of outcomes is possible. The analysis could be further strengthened by experimental measurement of depth- and time-dependent pH values in the SC following perturbation by topical application of either strong or weak electrolytes. Confocal Raman or fluorescence techniques with pH-sensitive probes might provide the requisite data.

Acknowledgments

KT was supported by the Procter & Gamble Company. GBK was supported by a grant from the US National Science Foundation (NSF) GOALI program under grant number 2124495 (CBET). Procter & Gamble is the industrial partner for this grant and JJ is the industrial PI.

CRediT author statement

Kevin Tonnis: Investigation, Formal Analysis, Visualization, Writing – Original draft preparation; **Joanna Jaworska:** Funding Acquisition, Supervision, Formal Analysis, Review and Editing; **Gerald Kasting:** Funding Acquisition, Supervision, Formal Analysis, Writing – Manuscript revision

Appendix: Mathematical model for weak electrolytes

A.1 SC and formulation pH

In Model 4.1, because the dose solution or vehicle is in intimate contact with the SC and may temporarily overwhelm its buffer capacity [17], the pH of the SC (pH_{sc}^{0}) is initially set to that of the vehicle (pH_{veh}^{0}). Here the superscript "0" represents time post-dose. Over time, both values are allowed to gradually return to the natural SC pH, herein designated $\mathrm{pH}_{sc}^{\infty}$, until the solvent comprising the vehicle has completely dissipated. The rate of return is governed by several factors including the buffer capacity of the applied dose (β_{dose}), the dissolution rate of any precipitated solid, and the loss of either free acid or free base by penetration or evaporation [17]. Here β_{dose} is defined as the number of nanomoles of strong acid or base required to bring the pH of the specific dose of test formulation (in μL·cm^{-2}) to $\mathrm{pH}_{\mathrm{sc}}^{\infty}$. For the case in which β_{dose} dominates the pH recovery kinetics we propose a first-order recovery with a rate constant k_r given by

$$k_r = \frac{a_0 \beta_{sc}}{\beta_{dose}} \tag{A1}$$

where β_{sc} is the effective buffer capacity of the SC for small doses of test formulation and a_0 is a proportionality constant related to the rate of resupply of protons to the SC. Miller and Kasting estimated β_{sc} to be 10-20 nmol cm^{-2}, we show below that $\alpha_0$has a value of about 2 h^{-1}, yielding $a_0\beta_{sc}$ values of approximately 20-40 nmol·cm^{-2}h^{-1}. *Note*: Although times here are expressed in h for convenience, all calculations are conducted with time in s for consistency with flux.

The combination of Eq. (A1) with the initial conditions described above leads to a pH drift in both the vehicle and the SC having the form

$$\mathrm{pH}_{veh}(t) = \mathrm{pH}_{sc}(t) = \mathrm{pH}_{\mathrm{sc}}^{\infty} + \Delta\mathrm{pH}^{0} \cdot e^{-k_r t} \quad \text{(A2)}$$

where

$$\Delta\mathrm{pH}^{0} = \mathrm{pH}_{veh}^{0} - \mathrm{pH}_{\mathrm{sc}}^{\infty} \quad \text{(A3)}$$

The half-life of the pH recovery process is thus

$$t_{1/2} = \frac{\ln(2)}{k_r} \quad \text{(A4)}$$

A.2 Transient governing equations

The evolution of the mass on the skin surface for each component *i* of the formulation is given by Eq. (A5):

$$\frac{-dM_{surf}^{i}}{dt} = J_{evap}^{i} + J_{sc}^{i} + J_{fol}^{i} \quad , i = 1, 2 \quad \text{(A5)}$$

where J_{evap}^{i} is the flux evaporating, $J_{sc}^{i}$is the flux entering the SC, and J_{fol}^{i} is the flux entering hair follicles. Here *i* = 1 represents the solute and *i* = 2 the solvent. Model 4.1 is limited to two diffusing species; hence the solute and solvent are treated as single components. An exception is made for precipitated solute on the skin surface as described in Sect. A.5. Because protonated and non-protonated forms of the solute can interconvert, it is convenient in Model 4.1 to express mass in moles rather than grams. This choice represents a departure from our earlier models. Thus, the units of all terms in Eq. (A5) are nmol·cm^{-2}s^{-1}. Although the general equation does not change throughout a simulated experiment, how each of the fluxes is calculated will change throughout dry down as the surface environment changes. For the remainder of this section we will omit the superscript *i* and consider only the fate of the solute (*i* = 1).

Yu et al. 2022 [9] imposed a surface roughness limitation to define how J_{fol} changes throughout the dry down process. If the vehicle is thicker than 25 µm, solutes are considered to be well mixed throughout the vehicle; thus they diffuse within the vehicle at an effectively infinite rate. The flux in this case is described by Yu et al 2021 [24]. But when the vehicle becomes thinner, J_{fol} drops abruptly to near zero because the solvent separates into discontinuous puddles. Permeants are no longer able to reach the entrance to the follicle unless they are directly above it.

A.3 Solute fully dissolved in the vehicle

While all solute is dissolved in the vehicle, the weak electrolyte will ionize based on the pH of the solvent. J_{sc} is defined so that the activity of the permeant in the vehicle is equal to that at the surface of the SC.

Ionized solute is assumed to have zero vapor pressure, so only the neutral solute can evaporate. The evaporation flux is given by [53]:

$$J_{evap} = k_{evap}\rho\left(\frac{a}{a_{sat}}\right) \quad \text{(A6)}$$

where a is the thermodynamic activity of the dissolved solute and a_{sat} its activity in a saturated solution. Here ρ is the solute density expressed in nmol·cm^{-3} and k_{evap} is the evaporation mass transfer coefficient (cm s^{-1}), given by [5]

$$k_{evap} = 10^3 \cdot \frac{k_g P_{vp}}{\rho RT} \quad \text{(A7)}$$

Here P_{vp} is in Pa, R = 8.314 J·mol^{-1}K^{-1} and T is temperature in K. The constant 10^3 adjusts for the mixture of SI and cgs units. The vapor pressure, P_{vp} (Pa), of the subcooled liquid is used for a dissolved solid. The gas phase mass transfer coefficient, k_g (cm s^{-1}), is given by [5]

$$k_g = \frac{1.756u^{0.78}}{\mathrm{MW}^{\frac{1}{3}}} \tag{A8}$$

where u is the ambient air flow rate in m·s^{-1}.

A.4 Saturated solution

As the solvent dries down, the concentration of the solute increases until it becomes saturated. Depending on the pH, the solubility of a weak electrolyte may be limited by the free acid or base or the corresponding salt. The total solubility of the solute in the vehicle, S_v, is given by Eq. (A9):

$$S_v = \min\left(S_{w\,salt}, \frac{Sw_{free}}{f_{non}}\right) \tag{A9}$$

where f_{non} is the nonionized fraction of the solute at the vehicle pH. Once the concentration reaches this limit, the solute will begin precipitating quickly enough to maintain saturation (no supersaturation is allowed in Model 4.1). The solute will penetrate and evaporate based on the ratio of the activity of the free (nonionized) permeant to its saturated activity. If the solubility is limited by the free permeant, this ratio will be unity. If it is limited by the salt solubility, the ratio will be less than 1 as the free solute remains undersaturated.

A.5 Only solid remains on skin surface

Once no more solvent remains on the surface of the skin, solute on the surface is no longer assumed to have continuous contact with the SC. The ratio of ionized to nonionized material is consequently no longer determined by the pH of the SC. Instead of tracking the total flux of a

permeant and calculating the amount of ionized and nonionized species based on the pH, deposited salt and free acid or base are tracked separately.

Yu et al. 2022 detail a model for predicting penetration of solids deposited on the surface of the skin [9]. In that model, the mass transfer of a deposited solid into the SC is limited by the rate of dissolution into and penetration through a thin lipid barrier with thickness δ_{lip} given by Eq. (A10):

$$J_{sc}(0,t) = \kappa_{lip}[K^{lip/w}S_w - \left(\frac{K^{lip/w}}{K^{sc/w}}\right)C_{sc}(0,t)] \quad \text{(A10)}$$

Here κ_{lip} is the mass transfer coefficient in the lipid layer (cm s^{-1}), S_w is the permeant's solubility in water (nmol·cm^{-3}), $K^{lip/w}$ is its lipid/water partition coefficient, $K^{sc/w}$ is its SC/water partition coefficient, and $C_{sc}(0,t)$ is the concentration at the top of the SC (nmol·cm^{-3}). For an in vitro experiment, the lipid barrier is assumed to have the properties of the SC lipids and κ_{lip} is determined as

$$\kappa_{lip} = \frac{k_{trans}\delta}{\delta_{lip}} f_{contact} \quad \text{(A11)}$$

where k_{trans} (cm s^{-1}) is the transverse mass transfer coefficient of the permeant across SC lipids and δ is the width of a single lipid bilayer, 13 nm or 1.3×10^{-6} cm [30]. The factor $f_{contact}$ is the fraction of the surface of the skin in contact with the solid. We note parenthetically that the secretion of sebum on the skin surface is likely to change the composition of the surface lipid film. This matter was considered by Yu et al. [9], who proposed an alternative to Eq. (A11) for in vivo exposures in which the SC lipid properties were replaced by those related to a skin surface lipid film comprised largely of sebaceous lipids. We refer the reader to Yu et al. for details.

Yu et al. 2022 used Eqs. (A10) and (A11) to describe a single solid on the skin surface. Because a deposited salt may have very different properties from its corresponding free acid or base, we treat each state of the deposited solid as a different species with the total flux given by the sum of the flux of each individual state:

$$J_{sc}(0,t) = f_{free}J(0,t)_{free} + \left(1 - f_{free}\right)J(0,t)_{salt} \quad \text{(A12)}$$

Here f_{free} is the fraction of solid on the skin surface that is free acid or base. This is analogous to the fraction nonionized in solution, f_{non}, which is used to determine the flux of a permeant dissolved in a vehicle. We assume that $K^{lip/w}$ for a salt will approach zero compared to a moderately lipophilic free acid or base, leading to $J(0,t) = 0$ for the salt form in Eq. (A10). Eq. (A12) can then be simplified to

$$\begin{aligned} J_{sc}(0,t) &= f_{free}J_{sc}(0,t)_{free} \\ &= f_{free}\kappa_{lip,free}\left[K_{free}^{lip/w}S_{w,free} - \left(\frac{K_{free}^{lip/w}}{K_{free}^{sc/w}}\right)f_{non,sc}C_{sc}(0,t)\right] \end{aligned} \quad \text{(A13)}$$

where $f_{non,sc}C_{sc}(0,t)$ gives the nonionized concentration at the top of the SC ($z = 0$).

We note at this point that the treatment of weak electrolytes as deposited solids on the skin surface differs from that when they are dissolved in the SC. On the surface, the free acid or base and its salt are treated as two distinct species, where in solution they are treated as one diffusing solute with pH-dependent properties. The f_{free} notation in the solid phase (rather than f_{non} as in solution) is introduced as a reminder that the solid species on the skin surface are not necessarily in equilibrium with each other, unlike ionized and nonionized species dissolved in an aqueous environment. We furthermore note that the simplification of Eq. (A12) to yield Eq. (A13)

means that we have invoked the pH-partition hypothesis at this step, i.e. we assume that only the nonionized form partitions into the lipid dissolution layer. This choice is discussed in Sect. 4.3.

The evaporation flux, J_{evap}, is calculated using Eqs. (A6) and (A7) as in the dissolved stages of dry down, except the vapor pressure of the solid is used instead of that of the subcooled liquid. As with the flux into the SC, the salt and free species are treated separately and added together to find the total flux. Most salts of weak electrolytes, including sodium benzoate and propranolol hydrochloride, have vapor pressures much lower than their corresponding free species, so the evaporation flux can be approximated as

$$J_{evap} = k_{evap_{free}} \rho \tag{A14}$$

where $k_{evap_{free}}$ is calculated from Eqs. (A7) and (A8) using the properties of the free acid or base.

Because free acids and bases will in general evaporate and penetrate more quickly than their corresponding salts, the fraction of salt on the surface will increase over time. Meanwhile, the pH in the SC will approach pH^{∞} according to Eqs. (A2) and (A3). Because the deposited solid and the SC are not in chemical equilibrium, a pH gradient and corresponding chemical potential gradient for protons will develop across the solid/SC interface. We postulate that a small proton flux through the lipid boundary layer, cf. Eqs. (A10) and (A11), will occur in response to this gradient. Although the contact between the deposited solid and the SC is not perfect, the ratio of salt and neutral species in the deposited solid will slowly drift toward the ratio within the SC as salt is converted to free acid or vise/versa. This is modeled by adding a proton flux term accounting for the conversion, J_{H+}, to Eqs. (A5), i.e.

$$\frac{dM_{free}}{dt} = J_{evap} + J_{sc} + J_{fol} + J_{H+} \quad \text{(A15)}$$

$$\frac{dM_{salt}}{dt} = J_{evap} + J_{sc} + J_{fol} - J_{H+} \quad \text{(A16)}$$

where J_{H+} is given by the equation

$$J_{H+} = \frac{a_1}{Z}(\mathrm{pH}_{sc} - \mathrm{pH}_{surf,eff}) \quad \text{(A17)}$$

Here a_1 (nmol cm^{-2}s^{-1}) is a to-be-determined proportionality constant, Z is the valence of the weak electrolyte, $\mathrm{pH}_{surf,eff}$ is the effective pH of the surface deposit based on the remaining amounts of free acid or base and salt. We estimate $\mathrm{pH}_{surf,eff}$ from the usual Henderson-Hasselbalch equation; thus

$$\mathrm{pH}_{surf,eff} = \mathrm{p}K_a + \log_{10}\left(\frac{1-f_{free}}{f_{free}}\right) \qquad \text{weak acid} \quad \text{(A18)}$$

$$\mathrm{pH}_{surf,eff} = \mathrm{p}K_a + \log_{10}\left(\frac{f_{free}}{1-f_{free}}\right) \qquad \text{weak base} \quad \text{(A19)}$$

The value of $\mathrm{pH}_{surf,eff}$ is limited to a maximum and minimum value based on the pH of solutions of pure free acid or base or pure salt. The calculation of these pH values is described in Sect. 2.3.1. The estimation of the constant, a_1, is discussed in Sect. 2.3.3.

The assertion of a proton flux, J_{H+}, across the lipid dissolution layer is an alternative to invoking another mechanism such as ion pairing that leads to absorption of deposited salt. We choose the proton flux alternative because it is a non-specific mechanism that applies to all weak electrolytes, and it is also consistent with our SC lipid permeability model that already allows ion transport via corneodesmosomes and/or lipid defects [14].

A.6. Only salt remains on surface

As the free acid or base depletes, eventually only salt is left on the surface. In this case, salt continues to convert to free permeant according to Eqs. (A15) and (A16). If the sum of fluxes of free permeant leaving the surface is greater than the flux converting from salt, free permeant will not accumulate, and because it cannot further deplete, $dM_{free}/dt = 0$. In this situation, according to Eq. (A15), the sum $J_{evap} + J_{sc} + J_{fol}$ must be balanced by J_{H+}. The split between evaporation and penetration is estimated based on the ratio of the fluxes that would be observed if M_{free} were greater than zero:

$$J_{evap_{free}} = \frac{J_{evap,max_{free}}}{J_{evap,max_{free}} + J_{sc,max_{free}}} \quad \text{(A20)}$$

$$J_{sc_{free}} = \frac{J_{sc,max_{free}}}{J_{evap,max_{free}} + J_{sc,max_{free}}} \quad \text{(A21)}$$

When a large dose of salt is applied (taken to be $M_{salt} \geq 50$ nmol·cm^{-2}), precipitated salt is considered to occlude the surface and prevent newly formed free acid or base from evaporating. In this case, the penetration flux, $J_{sc} + J_{fol}$, is equal to the conversion flux, J_{H+}.

References

[1] R.J. Scheuplein, L.W. Ross, Mechanism of percutaneous absorption V. Percutaneous absorption of solvent deposited solids, J. Invest. Dermatol., 62 (1974) 353-360.

[2] W.J. Albery, J. Hadgraft, Percutaneous absorption: theoretical description, J. Pharm. Pharmacol., 31 (1979) 129-139.

[3] R.H. Guy, J. Hadgraft, A theoretical description relating skin penetration to the thickness of the applied medicament, Int. J. Pharm., 6 (1980) 321-332.

[4] Y.G. Anissimov, M.S. Roberts, Diffusion modeling of percutaneous absorption kinetics: 2. Finite vehicle volume and solvent deposited solids, J. Pharm. Sci., 90 (2001) 504-520.

[5] G.B. Kasting, M.A. Miller, Kinetics of finite dose absorption through skin 2. Volatile compounds, J. Pharm. Sci., 95 (2006) 268-280.

[6] H.F. Frasch, A.M. Barbero, The transient dermal exposure: theory and experimental examples using skin and silicone membranes, J. Pharm. Sci., 97 (2008) 1578-1592.

[7] J.T. Carstensen, K. Danjo, S. Yoshioka, M. Uchiyama, Limits to the concept of solid-state stability, J. Pharm. Sci., 76 (1987) 548-550.

[8] J.T. Carstensen, A.L.W. Po, The state of water in drug decomposition in the moist solid state: Description and modeling, Int. J. Pharm., 83 (1992) 87-94.

[9] F. Yu, K. Tonnis, L. Xu, J. Jaworska, G.B. Kasting, Modeling the percutaneous absorption of solvent-deposited solids over a wide dose range, J. Pharm. Sci., 111 (2022) 769-779.

[10] K. Tonnis, J.M. Nitsche, L. Xu, A. Haley, J.S. Jaworska, G.B. Kasting, Impact of solvent dry down, vehicle pH and slowly reversible keratin binding on skin penetration of cosmetic relevant compounds: I. Liquids, Int. J. Pharm., 624 (2022) 122030.

[11] S.D. Roy, G.L. Flynn, Transdermal delivery of narcotic analgesics: pH, anatomical and subject influences on cutaneous permeability of fentanyl and sufentanyl, Pharm. Res., 7 (1990) 842-847.

[12] D. Chantasart, J. Hao, S.K. Li, Evaluation of skin permeation of beta-blockers for topical drug delivery, Pharm. Res., 30 (2013) 866-877.

[13] D. Chantasart, S. Chootanasoontorn, J. Suksiriworapong, S.K. Li, Investigation of pH Influence on skin permeation behavior of weak acids using nonsteroidal anti-inflammatory drugs, J. Pharm. Sci., 104 (2015) 3459-3470.

[14] G.B. Kasting, M.A. Miller, T.D. LaCount, J. Jaworska, A composite model for the transport of hydrophilic and lipophilic compounds across the skin, J. Pharm. Sci., 108 (2019) 337-349.

[15] N. Patel, J.F. Clarke, F. Salem, T. Abdulla, F. Martins, S. Arora, E. Tsakalozou, A. Hodgkinson, O. Arjmandi-Tash, S. Cristea, P. Ghosh, K. Alam, S.G. Raney, M. Jamei, S. Polak, Multi-phase multi-layer mechanistic dermal absorption (MPML MechDermA) model to predict local and systemic exposure of drug products applied on skin, CPT Pharmacometrics Syst Pharmacol., 00 (2022) 1-25.

[16] E. Tsakalozou, A. Babiskin, L. Zhao, Physiologically-based pharmacokinetic modeling to support bioequivalence and approval of generic products: a case for diclofenac sodium topical gel,1., CPT Pharmacomet Syst Pharmacol., 10 (2021) 399-411.

[17] M.A. Miller, G.B. Kasting, Absorption of solvent-deposited weak electrolytes and their salts through human skin in vitro, Int. J. Pharm., 620 (2022) 121753.

[18] X. Jin, M. Imran, Y. Mohammed, Topical semisolid products--Understanding the impact of metamorphosis on skin penetration and physicochemical properties, Pharmaceutics, 14 (2022) 2487.

[19] US FDA, FY2016 GDUFA Science and Research Report: Topical Dermatological Drug Products, Office of Generic Drugs, US FDA, Silver Springs, MD, 2016. URL: https://www.fda.gov/industry/generic-drug-user-fee-amendments/fy2016-regulatory-science-report-topical-dermatological-drug-products

[20] US FDA, FY2018 GDUFA Science and Research Report: Topical Dermatological Drug Products, Office of Generic Drugs, US FDA, Silver Springs, MD, 2018. URL: https://www.fda.gov/media/130622/download

[21] S. Raney, Bioequivalence of complex topical generics: in vitro and in vivo, Office of Generic Drugs, US FDA, Silver Springs, MD, 2020. URL: https://www.fda.gov/news-events/fda-meetings-conferences-and-workshops/bioequivalence-complex-topical-generics-vitro-and-vivo-10082020-10082020

[22] Advanced_Chemistry_Development, ACD/Labs Vers. EXP-20-BC4534-19, 2020.

[23] A. Klamt, COSMOthermX, Biovia Division, Dassault Systemes, Velizy-Villacoublay, France, 2020, Vers5274M, Solution thermodynamics program.

[24] F. Yu, K. Tonnis, G.B. Kasting, J. Jaworska, Computer simulation of skin permeability of hydrophobic and hydrophilic chemicals: Influence of follicular pathway, J. Pharm. Sci., 110 (2021) 2149-2156.

[25] R.M. Gajjar, M.A. Miller, G.B. Kasting, Evaporation of volatile organic compounds from human skin in vitro, Ann Occup Hyg, 57 (2013) 853-865.

[26] M.A. Miller, G.B. Kasting, Towards a better understanding of pesticide dermal absorption: diffusion model analysis of parathion absorption in vitro and in vivo, J. Toxicol. Environ. Health A., 73 (2010) 284-300.

[27] R.M. Gajjar, G.B. Kasting, Absorption of ethanol, acetone, benzene and 1,2-dichloroethane through human skin in vitro: a test of diffusion model predictions, Toxicol. Appl. Pharmacol., 281 (2014) 109-117.

[28] L. Xu, G.B. Kasting, Solvent and crystallization effects on the dermal absorption of hydrophilic and lipophilic compounds, J. Pharm. Sci., online in advance of print (2023), https://doi.org/10.1016/j.xphs.2023.09.025

[29] P.A. Sinko, Martin's Physical Pharmacy and Pharmaceutical Sciences, 6th ed., Lippincott Williams & Wilkins, Philadelphia, PA, 2011.

[30] T.-F. Wang, G.B. Kasting, J.M. Nitsche, A multiphase microscopic model for stratum corneum permeability. II. Estimation of physicochemical parameters and application to a large permeability database, J. Pharm. Sci., 96 (2007) 3024-3051.

[31] Y. Dancik, M.A. Miller, J. Jaworska, G.B. Kasting, Design and performance of a spreadsheet-based model for estimating bioavailability of chemicals from dermal exposure Adv. Drug Deliv. Revs., 65 (2013) 221-236.

[32] N. Otberg, H. Richter, S. H., U. Blume-Peytavi, W. Sterry, J. Lademann, Variations of hair follicle size and distribution in different body sites, J. Invest. Dermatol., 122 (2004) 14-19.

[33] J. Levin, H.I. Maibach, Human skin buffering capacity: an overview, Skin Res. Technol., 14 (2008) 121-126.

[34] H. Zhai, H.P. Chan, S. Farahmand, H.I. Maibach, Measuring human skin buffering capacity: an in vitro model, Skin Res. Technol., 15 (2009) 470-475.

[35] Y. Zheng, B. Sotoodian, W. Lai, H.I. Maibach, Buffering capacity of human skin layers: in vitro, Skin Res. Technol., 18 (2012) 114-119.

[36] P.R. Bevington, Data Reduction and Error Analysis for the Physical Sciences, McGraw-Hill, New York, 1969.

[37] OECD, Skin absorption: in vitro method, OECD Guidelines, 428 (2004).

[38] G.B. Kasting, M.A. Miller, V. Bhatt, A spreadsheet-based method for estimating the skin disposition of volatile compounds: application to N,N-diethyl-m-toluamide (DEET), Journal of Occupational and Environmental Hygiene, 10 (2008) 633-644.

[39] G.B. Kasting, Kinetics of finite dose absorption 1. Vanillylnonanamide, J. Pharm. Sci., 90 (2001) 202-212.

[40] S. Hawkins, B.R. Dasgupta, K.P. Ananthapadmanabhan, Role of pH in skin cleansing, Int. J. Cosmet. Sci., 43 (2021) 474-483.

[41] S. Stenzaly-Achtert, A. Schölermann, J. Schreiber, K.H. Diec, F. Rippke, S. Bielfeldt, Axillary pH and influence of deodorants, Skin Res. Technol., 6 (2008) 87-91.

[42] W.J. Moore, Physical Chemistry, 4th ed., Prentice-Hall, Englewood Cliffs, NJ, 1972, pp. 435-436.

[43] A.V. Rawlings, Molecular basis for stratum corneum maturation and moisturization, Brit J Dermatol, 171 Suppl 3 (2014) 19-28.

[44] X. Li, R. Johnson, B. Weinstein, E. Wilder, E. Smith, G.B. Kasting, Dynamics of water transport and swelling in human stratum corneum, Chem. Eng. Sci., 138 (2015) 164-172.

[45] J.J.H. Haftka, J.R. Parsons, H.A.J. Govers, Supercooled liquid vapour pressures and related thermodynamic properties of polycyclic aromatic hydrocarbons determined by gas chromatography, J. Chrom. A, 1135 (2006) 91-100.

[46] H.F. Frasch , A.L. Bunge, The transient dermal exposure II: post-exposure absorption and evaporation of volatile compounds, J. Pharm. Sci., 104 (2015) 1499-1507.

[47] J. Peress, Estimate evaporative losses from spills, Chem. Eng. Prog., (2003) 32-34.

[48] E.M. Sparrow, D.L. Misterek, Mass transfer at the base of a cylindrical cavity recessed in the floor of a flat duct, J Heat Transf-Trans ASME, 108 (1986) 853-859.

[49] M. Hiwada, T. Kawamura, Some characteristics of flow pattern and heat transfer past a circular cylindrical cavity, Bulletin of the JSME, 26 (1983) 1744.

[50] M.E.K. Kraeling, R.L. Bronaugh, In vitro percutaneous absorption of alpha hydroxy acids in human skin, J. Soc. Cosmet. Chem., 48 (1997) 187-197.

[51] M. Jiang, S.A. Quereshi, Assessment of in vitro percutaneous absorption of glycolic acid through human skin sections using a flow-through diffusion cell system, J. Dermatol. Sci., 18 (1998) 181-188.

[52] D. Gupta, D. Bhatia, V. Dave, V. Sutariya, S.V. Gupta, Salts of therapeutic agents: chemical, physicochemical, and biological considerations, Molecules, 23 (2018) 1719.

[53] M.A. Miller, G.B. Kasting, A spreadsheet-based method for simultaneously estimating the disposition of multiple ingredients applied to skin, J. Pharm. Sci., 104 (2015) 2047-2055.